Sound propagation in porous materials with annular pores

Massimiliano Nori, Rodolfo Venegas

Sound propagation in porous materials with annular pores

Massimiliano Nori[a)]
18 Via delle Mimose, 64025 Pineto, Teramo, Italy

Rodolfo Venegas
Université de Lyon, Ecole Nationale des Travaux Publics de l'Etat, Laboratoire Génie Civil et Bâtiment LGCB, Laboratoire de Tribologie et Dynamique des Systèmes LTDS UMR CNRS 5513, 1 Rue Maurice Audin, 69518 Vaulx-en-Velin, France

Long-wavelength sound propagation in porous materials with annular pores is investigated in this paper. Closed-form analytical expressions for the effective acoustical properties of this type of material were obtained. These are compared with both direct numerical calculations of the effective properties and their calculations obtained by using semi-phenomenological models. Analytical expressions for the input parameters of the latter, i.e., static viscous and thermal permeabilities, vis-cous and thermal characteristic lengths, and tortuosity, are also provided. The introduced model is successfully validated by comparing its predictions with measured data taken from literature. A parametric analysis that allows highlighting the influence of the different geometrical parameters of porous materials with annular pores on their sound absorptive properties is also presented.

I. INTRODUCTION

The solution of the problem of sound propagation in tubes of circular cross section saturated with a visco-thermal fluid has been derived by Kirchhoff[1] in the form of a complicated transcendental equation. This solution is of difficult application since it could only be solved for the wave number numerically. An approximated closed-form solution was presented by Zwikker and Kosten.[2] This solution, which has been obtained by decoupling and solving the equations of conservation of momentum and energy, is particularly attractive because of its simplicity when compared with Kirchhoff's full solution.[3,4] The validity of such a decoupled condition has been later justified using the two-scale asymptotic homogenization method for periodic media (see, for example, Ref. 5). Furthermore, the solution proposed in Ref. 2 provides almost identical result for broad ranges of frequency and tubes radii. In fact, its convergence to the exact solution derived by Kirchhoff has been first proven analytically by Weston[6] in the so-called narrow, wide, and very wide tube radius-frequency regions. The convergence in the intermediate region has been shown numerically in Ref. 3, using the Newton-Raphson method and a trapezoidal rule evaluation of the integral representation of Bessel function of first type to Kirchhoff's solution (see also Ref. 4). Since the assumptions leading to the decoupling of the equations of conservation of momentum and energy is based on are independent of the tube cross-section shape, Stinson[4] showed that it could be applied to tubes with arbitrary but constant cross-sectional shapes and provided a general procedure for calculating the effective permeability, bulk modulus, wave number, and characteristic impedance of the media. We will use this procedure in this paper.

This work investigates sound propagation in porous materials with annular pores, i.e., materials composed of an array of cylindrical circular pores with concentric solid cylinders. The aim of this paper is to provide closed-form analytical expressions for the long-wavelength effective acoustical properties, accounting for viscosity and heat transfer effects, of porous materials with annular pores. To the authors' knowledge, and as indicated in Ref. 7, these are not readily available. In addition, we provide analytical expressions for the so-called macroparameters (i.e., static viscous and thermal permeabilities, viscous and thermal characteristic lengths, and tortuosity[8–10]) of porous materials with annular pores.

A practical motivation of this study is that useful improvements in sound absorption of rigidly backed layers of a porous material with annular pores in comparison with that of a material with cylindrical pores with the same outer radius has been reported in Ref. 7. Sakamoto *et al.*[7] also calculated the wave number and characteristic impedance of an array of annular pores by using a model for an array of slit pores whose width was set equal to the distance between the outer and inner radii of the annular pores. They obtained a fairly good agreement between measured and predicted sound absorption coefficient. However, this was achieved by (i) using a model that does not directly correlate with the geometry of the material and (ii) correcting the layer thickness of the material in a somewhat arbitrary way.

In addition to Ref. 7, studies on oscillatory fluid flow and sound propagation in materials with annular tubes are relevant to our work. For example, oscillatory flow of an incompressible viscous fluid in a straight annular pipe was investigated in Ref. 11. The same problem but with the annular duct being saturated with a dusty incompressible fluid or

[a)]Electronic mail: massimiliano.nori.home@gmail.com

a Darcy-Brinkman medium has been studied in Refs. 12 and 13, respectively. Solute transport during oscillatory flow through an annular pipe with reactive walls was investigated in Ref. 14. A numerical investigation of sound propagation in moving media contained in an annular duct, with hard or soft walls, filled with an inviscid fluid has been published in Ref. 15 for mean uniform axial flow and for mean potential swirling flow in Ref. 16.

The paper is organized as follows. We solve the oscillatory fluid flow and heat conduction problems in an array of annular pores and calculate its long-wavelength effective acoustical properties from the respective analytical solutions in Sec. II A. The so-called macroparameters determining the asymptotic behavior of the effective acoustical properties are introduced in Sec. II B. The analytically calculated effective properties are then compared in Sec. III A with both (i) direct numerical calculations of the effective properties and (ii) their calculations obtained by using the semi-phenomenological models proposed in Refs. 8–10 in conjunction with the macroparameters introduced in this work. The model is then validated experimentally in Sec. III B using measured data published in Ref. 7. A parametric analysis of the model parameters focused on the sound absorptive properties of the material follows. The main results are summarized in the conclusions where we also suggest other potential applications of the results presented in this work.

II. THEORY

A. Model

Figure 1 depicts the geometry of the material investigated in this work. This corresponds to an array of annular pores of inner radius R_i and outer radius R. Their ratio is denoted as $\mathcal{R} = R_i/R$, while the annular pore width is given by $w = R - R_i = R(1-\mathcal{R})$. To simplify the presentation, we first consider a single annular pore. Plane sound waves propagate in the x-direction in the annular pore [see Fig. 1(c)]. The

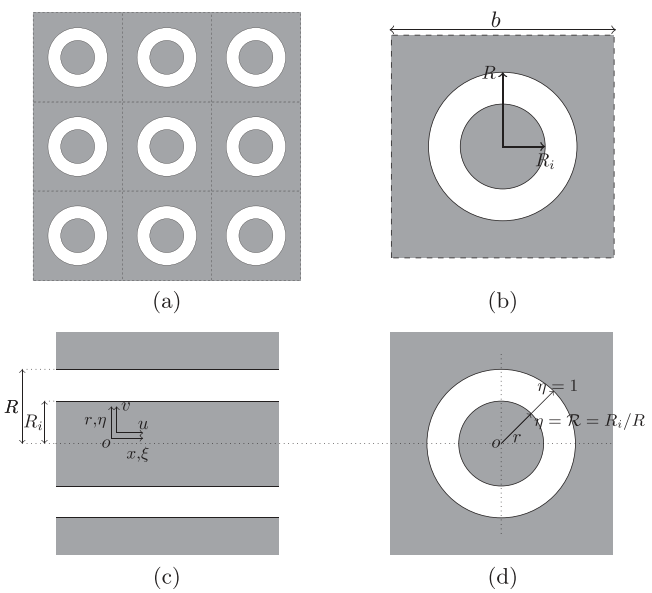

FIG. 1. (a) Geometry of an array of annular pores. (b) Unit cell (front view). (c) Side section of the unit cell and reference frame. (d) Normalized boundaries.

equations describing the motion of the fluid saturating the annular pore are the Navier-Stokes equation with a constant-value viscosity μ [Eqs. (1), (2)], the continuity equation [Eq. (3)], the equation of state for an ideal gas Eq. (4), and the energy balance Eq. (5),

$$\bar{\rho}\left(\frac{\partial \bar{u}}{\partial t} + \bar{v}\frac{\partial \bar{u}}{\partial r} + \bar{u}\frac{\partial \bar{u}}{\partial x}\right) = -\frac{\partial \bar{p}}{\partial x} + \mu\left(\frac{\partial^2 \bar{u}}{\partial x^2} + \frac{\partial^2 \bar{u}}{\partial r^2} + \frac{1}{r} \times \frac{\partial \bar{u}}{\partial r} + \frac{1}{3}\frac{\partial}{\partial x}\left(\frac{\partial \bar{u}}{\partial x} + \frac{\partial \bar{v}}{\partial r} + \frac{\bar{v}}{r}\right)\right), \tag{1}$$

$$\bar{\rho}\left(\frac{\partial \bar{v}}{\partial t} + \bar{v}\frac{\partial \bar{v}}{\partial r} + \bar{u}\frac{\partial \bar{v}}{\partial x}\right) = -\frac{\partial \bar{p}}{\partial r} + \mu\left(\frac{\partial^2 \bar{v}}{\partial r^2} + \frac{1}{r}\frac{\partial \bar{v}}{\partial r} - \frac{\bar{v}}{r^2} + \frac{\partial^2 \bar{v}}{\partial x^2} + \frac{1}{3}\frac{\partial}{\partial r}\left(\frac{\partial \bar{u}}{\partial x} + \frac{\partial \bar{v}}{\partial r} + \frac{\bar{v}}{r}\right)\right), \tag{2}$$

$$\frac{\partial \bar{\rho}}{\partial t} + \bar{u}\frac{\partial \bar{\rho}}{\partial x} + \bar{v}\frac{\partial \bar{\rho}}{\partial r} + \bar{\rho}\left(\frac{\partial \bar{u}}{\partial x} + \frac{\partial \bar{v}}{\partial r} + \frac{\bar{v}}{r}\right) = 0, \tag{3}$$

$$\bar{p} = \bar{\rho} R_0 \bar{T}, \tag{4}$$

$$\bar{\rho} C_p\left(\frac{\partial \bar{T}}{\partial t} + \bar{u}\frac{\partial \bar{T}}{\partial x} + \bar{v}\frac{\partial \bar{T}}{\partial r}\right) = \kappa\left(\frac{\partial^2 \bar{T}}{\partial r^2} + \frac{1}{r}\frac{\partial \bar{T}}{\partial r} + \frac{\partial^2 \bar{T}}{\partial x^2}\right) + \frac{\partial \bar{p}}{\partial t} + \bar{u}\frac{\partial \bar{p}}{\partial x} + \bar{v}\frac{\partial \bar{p}}{\partial r} + \Phi_v, \tag{5}$$

with

$$\frac{\Phi_v}{\mu} = 2\left(\left(\frac{\partial \bar{u}}{\partial x}\right)^2 + \left(\frac{\partial \bar{v}}{\partial r}\right)^2 + \left(\frac{\bar{v}}{r}\right)^2\right) + \left(\frac{\partial \bar{v}}{\partial x} + \frac{\partial \bar{u}}{\partial r}\right)^2 - \frac{2}{3}\left(\frac{\partial \bar{u}}{\partial x} + \frac{\partial \bar{v}}{\partial r} + \frac{\bar{v}}{r}\right)^2. \tag{6}$$

Equations (1)–(5) suffice to obtain the solution for the same number of unknown quantities, i.e., the velocities in the axial $\bar{u}$ and radial directions $\bar{v}$, density $\bar{\rho}$, temperature $\bar{T}$, and pressure $\bar{p}$.

The main assumptions involved in sound propagation through the materials under investigation are those described in Ref. 17. (a) The wavelength and any local characteristic size of the material, e.g., $w = R_i - R$, are larger than the molecular mean free path ℓ. For air at normal pressure and temperature conditions, this condition breaks down for frequencies in the order of 10^8 Hz or when $w = O(\ell) \approx 60$ nm. (b) No steady flow. (c) Small amplitude sinusoidal perturbations (neither circulation nor turbulence). (d) The length of the annular pore is long enough so that end effects are negligible.

Equations (1)–(6) can be linearized and made dimensionless by following the approach in Ref. 3. First, the variables are written as follows: $\bar{u} = c_0 u(x,r)e^{j\omega t}$, $\bar{v} = c_0 v(x,r)e^{j\omega t}$, $\bar{p} = P_0(1 + p(x,r)e^{j\omega t}) = (\rho_0 c_0^2/\gamma)(1 + p(x,r)e^{j\omega t})$, $\bar{\rho} = \rho_0(1 + \rho(x,r)e^{j\omega t})$, $\bar{T} = T_0(1 + T(x,r)e^{j\omega t})$, $\eta = r/R$, $\xi = \omega x/c_0$, $\tau = \omega t$, $k = \omega R/c_0 = k_0 R$. Here, ω is the angular frequency;

$c_0 = \sqrt{\gamma P_0/\rho_0}$ is the speed of sound in the saturating fluid; P_0, ρ_0, and T_0 are the equilibrium pressure, density, and temperature; and γ is the heat capacity ratio.

Replacing the variables into Eqs. (1)–(6) and retaining only linear terms lead to

$$ju = \frac{1}{s_v^2}\left(\frac{\partial^2 u}{\partial \eta^2} + \frac{1}{\eta}\frac{\partial u}{\partial \eta}\right) - \frac{1}{\gamma}\frac{\partial p}{\partial \xi}, \tag{7}$$

$$\frac{\partial p}{\partial \eta} = 0, \tag{8}$$

$$j\rho = -\frac{1}{k}\left(k\frac{\partial u}{\partial \xi} + \frac{\partial v}{\partial \eta} + \frac{v}{\eta}\right), \tag{9}$$

$$p = \rho + T, \tag{10}$$

$$jT = \frac{1}{s_t^2}\left(\frac{\partial^2 T}{\partial \eta^2} + \frac{1}{\eta}\frac{\partial T}{\partial \eta}\right) + \frac{\gamma - 1}{\gamma} jp. \tag{11}$$

Here the shear s_v and thermal s_t wave numbers are defined as $s_v = R/\delta_v$ and $s_t = R/\delta_t$, where $\delta_v = \sqrt{\mu/\rho_0\omega}$ and $\delta_t = \sqrt{\kappa/\rho_0 C_p \omega}$ are the viscous and thermal boundary layer thicknesses, respectively. These are related through $\delta_v = \sqrt{\mathrm{Pr}}\delta_t$, where $\mathrm{Pr} = C_p\mu/\kappa$ is the Prandtl number and C_p and κ are the isobaric specific heat capacity and the thermal conductivity of the saturating fluid.

In deriving Eqs. (7)–(11), it has been also assumed that (i) the annular pore outer radius is smaller than the wavelength, i.e., $k_0 R \ll 1$, and (ii) the radial velocity component v is much smaller than the axial velocity component u.

To obtain the solution of Eqs. (7) and (11), the following boundary conditions and assumptions are considered.

No-slip condition is set on the wall surfaces, i.e.,

$$u(\eta = \mathcal{R}) = u(\eta = 1) = v(\eta = \mathcal{R}) = v(\eta = 1) = 0. \tag{12}$$

Assuming that the volumetric heat capacity of the saturating fluid is much smaller than that of the walls, the isothermal boundary condition for temperature on the wall surfaces holds,

$$T(\eta = \mathcal{R}) = T(\eta = 1) = 0. \tag{13}$$

Note that these two boundary conditions are valid as long as the distance $w = R - R_i$ is much larger than the molecular mean free path. When $w = O(\ell)$, effects related to the molecular nature of the gas start becoming considerable[18–20] and the boundary conditions (12) and (13) should be replaced by the slip and temperature-jump boundary conditions, respectively (see, for example, Eqs. 3a and 3b in Ref. 18).

Equation (7) can be solved using the method of separation of variables. To do so, the axial velocity is written as $u = f(\xi)h(z)$ with $z = j^{3/2}\eta s_v$. This leads to the following non-homogeneous Bessel equation of order zero:

$$\frac{\partial^2 h(z)}{\partial z^2} + \frac{1}{z}\frac{\partial h(z)}{\partial z} + h(z) = \frac{1}{f(\xi)}\frac{j}{\gamma}\frac{\partial p}{\partial \xi}.$$

The solution of this equation is given by[21]

$$h(z) = A_1 J_0(z) + A_2 Y_0(z) + \frac{1}{f(\xi)}\frac{j}{\gamma}\frac{\partial p}{\partial \xi}, \tag{14}$$

where J_0 and Y_0 are Bessel functions of the first and second kind of order zero. The constants A_1 and A_2 are determined by using the no-slip boundary condition (12) and noting that $h(j^{3/2}s_v) = 0$ and $h(j^{3/2}s_v\mathcal{R}) = 0$. These are given by

$$A_1 = -\frac{1}{f(\xi)}\frac{j}{\gamma}\frac{\partial p}{\partial \xi}\Theta_J(s_v, \mathcal{R}), \tag{15}$$

$$A_2 = -\frac{1}{f(\xi)}\frac{j}{\gamma}\frac{\partial p}{\partial \xi}\Theta_Y(s_v, \mathcal{R}), \tag{16}$$

where

$$\Theta_J(s_v, \mathcal{R}) = \frac{\Xi^{-1}(s_v, \mathcal{R})}{J_0\left(j^{3/2}s_v\right)}\left(1 - \frac{Y_0\left(j^{3/2}s_v\right)}{Y_0\left(j^{3/2}s_v\mathcal{R}\right)}\right), \tag{17}$$

$$\Theta_Y(s_v, \mathcal{R}) = \frac{\Xi^{-1}(s_v, \mathcal{R})}{Y_0\left(j^{3/2}s_v\mathcal{R}\right)}\left(1 - \frac{J_0\left(j^{3/2}s_v\mathcal{R}\right)}{J_0\left(j^{3/2}s_v\right)}\right), \tag{18}$$

$$\Xi(s_v, \mathcal{R}) = 1 - \frac{Y_0\left(j^{3/2}s_v\right)}{Y_0\left(j^{3/2}s_v\mathcal{R}\right)}\frac{J_0\left(j^{3/2}s_v\mathcal{R}\right)}{J_0\left(j^{3/2}s_v\right)}. \tag{19}$$

The velocity is then given by

$$u(\xi, \eta) = \frac{j}{\gamma}\frac{\partial p}{\partial \xi}\Big(1 - J_0\left(j^{3/2}\eta s_v\right)\Theta_J(s_v, \mathcal{R}) - Y_0\left(j^{3/2}\eta s_v\right)\Theta_Y(s_v, \mathcal{R})\Big). \tag{20}$$

When $\mathcal{R} = R_i/R \to 0$, one obtains that $\Theta_J(s_v, \mathcal{R} \to 0) = J_0^{-1}(j^{3/2}s_v)$ and $\Theta_Y(s_v, \mathcal{R} \to 0) = 0$. Hence, the fluid velocity in a cylindrical pore[3] is retrieved.

Equations (11) and (13) are formally identical to Eqs. (7) and (12). The differences are that s_v is replaced by s_t and the forcing term is changed from $f_1 = (1/\gamma)(\partial p/\partial \xi)$ to $f_2 = j[(\gamma - 1)/\gamma]p$. The solutions are therefore related by a factor f_1/f_2, i.e., $u(\chi, \eta, s_t)/T(\chi, \eta, s_t) = f_1/f_2$. The temperature is given by

$$T(\xi, \eta) = \frac{\gamma - 1}{\gamma} p\Big(1 - J_0\left(j^{3/2}\eta s_t\right)\Theta_J(s_t, \mathcal{R}) - Y_0\left(j^{3/2}\eta s_t\right)\Theta_Y(s_t, \mathcal{R})\Big). \tag{21}$$

The density is now written in terms of pressure and known temperature using Eq. (4) as $\rho = p(1 - T/p)$. Hence the mass balance Eq. (9) can be rewritten as

$$\frac{\partial(\eta v)}{\partial \eta} = -k\left(jp\left(\eta - \eta\frac{T}{p}\right) + \frac{\partial(\eta u)}{\partial \xi}\right). \tag{22}$$

The integration of this equation with respect to η yields

$$\eta v - F(\xi) = -k\left(jp\left(\frac{\eta^2}{2} - \frac{1}{p}\int \eta T d\eta\right) + \frac{\partial}{\partial \xi}\int \eta u d\eta\right). \tag{23}$$

Here $F(\xi)$ is an integration constant and the integrals on the right-hand side are given by

$$\mathcal{U}(\eta,\xi) = \int \eta u d\eta = \frac{j}{\gamma}\frac{\partial p}{\partial \xi}\left(\frac{\eta^2}{2} - \Theta_J(s_v,\mathcal{R}) \times \frac{\eta J_1\left(j^{3/2}s_v\eta\right)}{j^{3/2}s_v} - \Theta_Y(s_v,\mathcal{R})\frac{\eta Y_1\left(j^{3/2}s_v\eta\right)}{j^{3/2}s_v}\right), \tag{24}$$

$$\mathcal{T}(\eta,\xi) = \int \eta T d\eta = \frac{\gamma-1}{\gamma}p\left(\frac{\eta^2}{2} - \Theta_J(s_t,\mathcal{R}) \times \frac{\eta J_1\left(j^{3/2}s_t\eta\right)}{j^{3/2}s_t} - \Theta_Y(s_t,\mathcal{R})\frac{\eta Y_1\left(j^{3/2}s_t\eta\right)}{j^{3/2}s_t}\right). \tag{25}$$

Applying the no-slip boundary condition (12), the mass balance equations becomes

$$-F(\xi) = -k\left(jp\left(\frac{1}{2} - \frac{1}{p}\mathcal{T}(1,\xi)\right) + \frac{\partial}{\partial\xi}\mathcal{U}(1,\xi)\right), \tag{26}$$

$$-F(\xi) = -k\left(jp\left(\frac{\mathcal{R}^2}{2} - \frac{1}{p}\mathcal{T}(\mathcal{R},\xi)\right) + \frac{\partial}{\partial\xi}\mathcal{U}(\mathcal{R},\xi)\right). \tag{27}$$

Subtracting these equations one obtains the following equation:

$$\frac{2}{1-\mathcal{R}^2}\frac{\partial}{\partial\xi}\left(\mathcal{U}(\mathcal{R},\xi) - \mathcal{U}(1,\xi)\right) = jp\left(1 + \frac{1}{p}\frac{2}{1-\mathcal{R}^2}\left(\mathcal{T}(\mathcal{R},\xi) - \mathcal{T}(1,\xi)\right)\right). \tag{28}$$

Evaluating Eqs. (24) and (25) at $\eta = \mathcal{R}$ and $\eta = 1$, replacing the result into Eq. (28), and reminding that $\eta = \omega x/c_0$, lead to the following wave equation:

$$\frac{\widehat{\mathcal{K}}(\omega)}{\mu}\frac{\partial^2 p}{\partial x^2} = \frac{j\omega p}{\widehat{E}(\omega)}, \tag{29}$$

where $\widehat{\mathcal{K}}(\omega)$ and $\widehat{E}(\omega)$ are the dynamic viscous permeability and bulk modulus of a single annular pore. These are given by

$$\widehat{\mathcal{K}}(\omega) = \chi(s_v), \tag{30}$$

$$\widehat{E}(\omega) = \frac{P_0}{1 - j\omega\rho_0 C_p\dfrac{\gamma-1}{\gamma}\dfrac{\widehat{\theta}(\omega)}{\kappa}}, \tag{31}$$

where the dynamic thermal permeability $\widehat{\theta}(\omega)$ is given by

$$\widehat{\theta}(\omega) = \chi(s_t) = \chi(s_v\sqrt{\mathrm{Pr}}) = \widehat{\mathcal{K}}(\omega\mathrm{Pr}), \tag{32}$$

and the function χ reads

$$\chi(s) = -j\frac{R^2}{s^2}\left(1 - \frac{1}{1-\mathcal{R}^2}\frac{2}{j^{3/2}s}J_1\left(j^{3/2}s\right)\Theta_J(s,\mathcal{R}) \times \left(1 - \frac{j^{3/2}s\mathcal{R}J_1\left(j^{3/2}s\mathcal{R}\right)}{j^{3/2}sJ_1\left(j^{3/2}s\right)}\right) - \frac{1}{1-\mathcal{R}^2}\frac{2}{j^{3/2}s} \times Y_1\left(j^{3/2}s\right)\Theta_Y(s,\mathcal{R})\left(1 - \frac{j^{3/2}s\mathcal{R}Y_1\left(j^{3/2}s\mathcal{R}\right)}{j^{3/2}sY_1\left(j^{3/2}s\right)}\right)\right). \tag{33}$$

Note that Θ_J and Θ_Y are given Eqs. (17) and (18), respectively [see also Eq. (19)].

For a bulk material with porosity ϕ, defined as the ratio between the volume occupied by the fluid and the total volume of the material, the terms $\widehat{\mathcal{K}}(\omega)$ and $\widehat{E}(\omega)$ in Eq. (29) are replaced by $\mathcal{K}(\omega)$ and $E(\omega)$, respectively. These are given by

$$\mathcal{K}(\omega) = \phi\widehat{\mathcal{K}}(\omega), \tag{34}$$

$$E(\omega) = \frac{P_0}{\phi\left(1 - j\omega\rho_0 C_p\dfrac{\gamma-1}{\gamma}\dfrac{\theta(\omega)}{\phi\kappa}\right)}, \tag{35}$$

with

$$\theta(\omega) = \phi\widehat{\theta}(\omega). \tag{36}$$

These expressions are valid for any type of annular pores arrangement, e.g., square, hexagonal, triangular lattice; provided that any local characteristic size is much smaller than the wavelength. One such a local characteristic size can be the separation distance between the annular pores. For example, if the annular pores are arranged in a square lattice with cell size b (see Fig. 1) and porosity $\phi = \pi R^2(1-\mathcal{R}^2)/b^2$, the separation distance is estimated by $b - 2R$ and should be much smaller than the wavelength.

The speed of sound $\mathcal{C}$ in the bulk material, and its characteristic impedance Z_c and wave number k_c are given by[22]

$$Z_c(\omega) = \sqrt{\frac{\mu}{j\omega\mathcal{K}(\omega)}E(\omega)}, \tag{37}$$

$$k_c(\omega) = \omega\sqrt{\frac{\mu}{j\omega\mathcal{K}(\omega)}\frac{1}{E(\omega)}}, \tag{38}$$

$$\mathcal{C}(\omega) = \frac{\omega}{k_c(\omega)} = \sqrt{\frac{j\omega\mathcal{K}(\omega)}{\mu}E(\omega)}. \tag{39}$$

The theory will be validated by comparing the predictions of the analytical model with measurements of sound absorption coefficient $\alpha(\omega)$ of a rigidly backed layer of material with thickness d. The sound absorption coefficient is related to the pressure reflection coefficient R_e and surface impedance Z_w through the following expressions (with $Z_0 = \rho_0 c_0$ being the characteristic impedance of the saturating fluid):[22]

$$\alpha(\omega) = 1 - |R_e|^2, \quad R_e(\omega) = \frac{Z_w - Z_0}{Z_w + Z_0}, \quad \text{and}$$
$$Z_w(\omega) = -jZ_c\cot(k_c d). \tag{40}$$

B. Macroparameters and semi-phenomenological models

Analytical expressions for the input parameters of the semi-phenomenological models proposed in Refs. 8 and 10 are introduced in this section for porous materials with annular pores. These parameters correspond to the static viscous $\mathcal{K}_0$ and thermal θ_0 permeabilities, the viscous Λ and thermal Λ' characteristic lengths, and tortuosity α_∞. Their definition can be found in Refs. 8 and 10.

The static viscous $\mathcal{K}_0$ and thermal θ_0 permeabilities are calculated from the solution of Eqs. (7) and (12), and Eqs. (11) and (13) for $\omega = 0$. These are given by

$$\mathcal{K}_0 = \theta_0 = \phi\frac{R^2}{8}f(\mathcal{R}), \tag{41}$$

where the function f satisfies $f(\mathcal{R}\to 0) = 1$ and $f(\mathcal{R}\to 1) = 0$, and is given by

$$f(\mathcal{R}) = 1 + \mathcal{R}^2 - \frac{1-\mathcal{R}^2}{\ln(1/\mathcal{R})}. \tag{42}$$

As discussed in Sec. II A, the distance w can become comparable with the molecular mean free path when $\mathcal{R}\to 1$ and, in such a case, rarefaction effects should be accounted for. The permeability values given by Eq. (41) when $\mathcal{R}$ approaches unity should be considered as mathematical instead of physical limiting values.

Since the velocity of an inviscid fluid saturating the annular pores is constant, one can directly assess the tortuosity of the material from its definition (see Eq. 2.9 in Ref. 8). Following the same argument, the viscous characteristic length Λ is calculated from its definition (see Eq. 2.17 in Ref. 8) and coincides with the thermal characteristic length Λ'. These parameters read

$$\alpha_\infty = 1 \quad \text{and} \quad \Lambda = \Lambda' = Rg(\mathcal{R}), \tag{43}$$

where the function g tends to 1 when $\mathcal{R}\to 0$ and is given by

$$g(\mathcal{R}) = 1 - \mathcal{R}. \tag{44}$$

Note that the macroparameters for an array of cylindrical pores are retrieved when $\mathcal{R}\to 0$.

The viscous[8] and thermal[10] characteristic frequencies, i.e., $\omega_v = \mu\phi/\alpha_\infty\rho_0\mathcal{K}_0$ and $\omega_t = \kappa\phi/\rho_0 C_p\theta_0$, determining the transition from viscosity to inertia-dominated and isothermal to adiabatic sound propagation are given by

$$\frac{\omega_v}{\omega_v(\mathcal{R}=0)} = \frac{\omega_t}{\omega_t(\mathcal{R}=0)} = \frac{1}{f(\mathcal{R})}, \tag{45}$$

where $\omega_v(\mathcal{R}=0) = 8\mu/\rho_0 R^2$ and $\omega_t(\mathcal{R}=0) = 8\kappa/\rho_0 C_p R^2$ correspond to the characteristic frequencies for an array of cylindrical pores. Since $f(\mathcal{R}) < 1\ \forall\mathcal{R}$, one can conclude that introducing concentric solid cylinders in the pores leads to higher characteristic frequencies. This is due to the reduction of the separation distance between the pore walls.

The viscous[8] and thermal[10] shape factors are, respectively, defined by $M_v = 8\mathcal{K}_0\alpha_\infty/\phi\Lambda^2$ and $M_t = 8\theta_0/\phi\Lambda'^2$. For the materials under study, these are given by

$$\frac{M_v}{M_v(\mathcal{R}=0)} = \frac{M_t}{M_t(\mathcal{R}=0)} = \frac{f(\mathcal{R})}{g^2(\mathcal{R})}, \tag{46}$$

where $M_v(\mathcal{R}=0) = M_t(\mathcal{R}=0) = 1$ are the shape factors for an array of cylindrical pores. The limiting values of the shape factors are $M_v(\mathcal{R}\to 0) = M_t(\mathcal{R}\to 0) = 1$ and $M_v(\mathcal{R}\to 1) = M_t(\mathcal{R}\to 1) = 2/3$.

These macroparameters can be used to calculate the dynamic viscous and thermal permeabilities using the following semi-phenomenological models:[8,10]

$$\mathcal{K}(\omega) = \mathcal{X}(\omega,\mathcal{K}_0,\omega_v,M_v) \quad \text{and} \quad \theta(\omega) = \mathcal{X}(\omega,\theta_0,\omega_t,M_t), \tag{47}$$

where

$$\mathcal{X}(\omega,\mathcal{X}_0,\varpi,\mathcal{M}) = \mathcal{X}_0\left(\frac{j\omega}{\varpi} + \sqrt{1+\frac{j\omega}{\varpi}\frac{\mathcal{M}}{2}}\right)^{-1}. \tag{48}$$

The results obtained with these semi-phenomenological models will be compared in Sec. III with the analytical models as well as the respective effective parameters numerically calculated from the solution of the oscillatory Stokes and heat conduction problems.

C. Analysis of the characteristic impedance and wave number

The behavior of $\mathcal{K}$ is characterized by the viscous characteristic frequency ω_v. Considering leading-order terms only, the dynamic permeability varies from[8] $\mathcal{K}(\omega\ll\omega_v)\approx\mathcal{K}_0$ to $\mathcal{K}(\omega\gg\omega_v)\approx -j\phi\delta_v^2/\alpha_\infty$. Similarly, the low- and high-frequency asymptotic values of the dynamic thermal permeability are[10] $\theta(\omega\ll\omega_t)\approx\theta_0$ and $\theta(\omega\gg\omega_t)\approx -j\phi\delta_t^2$. Hence the dynamic bulk modulus varies from $E(\omega\ll\omega_t)\approx P_0/\phi(1-(\gamma-1)j\omega/\omega_t\gamma)\approx P_0/\phi$ to $E(\omega\gg\omega_t)\approx\gamma P_0/\phi$. Then, the characteristic impedance takes the following limiting values: $Z_c(\omega\ll\omega_v) = Z_{c0}\approx\sqrt{\mu P_0/j\omega\phi\mathcal{K}_0}$ and $Z_c(\omega\gg\omega_v) = Z_{c\infty}\approx\rho_0 c_0\sqrt{\alpha_\infty}/\phi$. In turn, the wave number tends to $k_c(\omega\ll\omega_v) = k_{c0}\approx\omega\sqrt{\mu\phi/j\omega\mathcal{K}_0 P_0}$ and $k_c(\omega\gg\omega_v) = k_{c\infty}\approx\omega\sqrt{\alpha_\infty}/c_0$. These general expressions show that the low-frequency acoustic behavior of single porosity porous materials is determined by the porosity ϕ, static viscous permeability $\mathcal{K}_0$, equilibrium pressure, and dynamic viscosity. In particular, materials having pores with constant cross-section shape (e.g., cylindrical, triangular, slit, annular) and the same values of ϕ and $\mathcal{K}_0$ possess very similar acoustical properties at low frequencies as well as high frequencies since for this type of materials $\alpha_\infty = 1$.

Using Eqs. (41) and (43), one obtains that the characteristic impedance and wave number of porous materials with annular pores tend to

$$\frac{Z_{c0}}{Z_{c0}(\mathcal{R}=0)} = \frac{k_{c0}}{k_{c0}(\mathcal{R}=0)} \approx \sqrt{\frac{1}{f(\mathcal{R})}}, \tag{49}$$

$$\frac{Z_{c\infty}}{Z_{c\infty}(\mathcal{R}=0)} = \frac{k_{c\infty}}{k_{c\infty}(\mathcal{R}=0)} \approx 1, \tag{50}$$

where $Z_{c0}(\mathcal{R}=0) \approx \sqrt{8\mu P_0/j\omega\phi^2 R^2}$, $Z_{c\infty}(\mathcal{R}=0) \approx \rho_0 c_0/\phi$, $k_{c0}(\mathcal{R}=0) \approx \omega\sqrt{8\mu/j\omega P_0 R^2}$, and $k_{c\infty}(\mathcal{R}=0) \approx \omega/c_0$.

Equation (49) shows that the low-frequency magnitude of the real and imaginary parts of the characteristic impedance and wave number of a material with annular pores are larger than those of a material with cylindrical pores with the same porosity ϕ and outer radius R. As a consequence, higher sound attenuation and slower speed of sound in the material with annular pores $\forall\mathcal{R}$ is observed at low frequencies. At high frequencies, both type of materials present, to the leading order, the same acoustical properties, as shown by Eq. (50).

III. RESULTS AND DISCUSSION

A. Comparison between analytical, semi-phenomenological, and numerical models

Figure 2 compares the analytically calculated function $f(\mathcal{R})$ and the ratio between the static viscous and thermal permeability of the array of annular pores and those of an array of cylindrical pores. In the same figure, the function $g(\mathcal{R})$ is compared to the ratio between the viscous characteristic length of the array of annular pores and that of an array of cylindrical pores. The numerical results have been obtained from the solution of the static fluid flow [Eqs. (7) and (12) for $\omega=0$], heat conduction [Eqs. (11) and (13) for $\omega=0$], and inviscid fluid flow [Eqs. (7), (8), and (12) for $\omega\to\infty$] problems. The resolution of the problems was performed using the finite element method. A good agreement between the analytical and numerical calculations is observed and the equality between the static permeabilities is confirmed. Moreover, the equality of the characteristic lengths [see Eq. (43)] is also verified.

The inset plot shows the permeability ratios $\mathcal{K}_0/\mathcal{K}_0^{slit}$ and $\mathcal{K}_0/\mathcal{K}_0^{rect}$. The static viscous permeabilities $\mathcal{K}_0$, $\mathcal{K}_0^{slit}$, and $\mathcal{K}_0^{rect}$, respectively, correspond to that of an array of (i) annular pores, (ii) slit pores[7] with width $2h=w$, and (iii) rectangular pores[4] with sides $2a=w$ and $2b=\pi R^2(1-\mathcal{R}^2)/2a$. All these arrays have the same porosity and, in particular, the rectangular pores have the same cross-section area as that of the annular pores. The static viscous permeability of an array of annular pores is larger than that of an array of slit or rectangular pores $\forall\mathcal{R}$. However, $\mathcal{K}_0$ can be well approximated by either $\mathcal{K}_0^{slit}$ or $\mathcal{K}_0^{rect}$ when $\mathcal{R}$ is larger than approximately 0.5 and 0.95, respectively. Considering the significant influence of the static viscous permeability on the characteristic impedance and wave number of single porosity materials at low frequencies (see Sec. II C), one can conclude that the acoustical properties of an array of annular pores are similar to those of an array of slit or rectangular pores having the geometrical parameters discussed in this paragraph only when $\mathcal{R}$ is larger than the quoted values.

Figure 3 shows the normalized dynamic viscous permeability $\mathcal{K}(\omega)/\mathcal{K}_0$ of an array of annular pores with $R=500\,\mu$m, $\mathcal{R}=0.5$, and $\phi=0.3$. The analytical model for this quantity, i.e., Eq. (34), is compared with both its calculation obtained by using the semi-phenomenological model Eq. (47) and the parameters derived in Sec. II B, and its direct numerical calculation obtained from the solution of Eqs. (7) and (12) for a discrete set of frequencies. An excellent agreement is observed between the calculations obtained with the different models. Note that the normalized dynamic viscous permeability of an array of cylindrical pores (with $R=500\,\mu$m and $\phi=0.3$) is also plotted. It is clear that its associated viscous characteristic frequency is smaller than that of the array of annular pores, as predicted by Eq. (45).

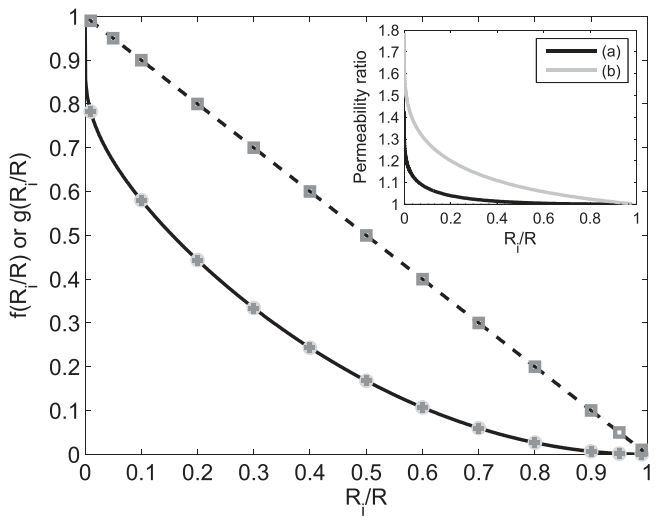

FIG. 2. Dependence of the functions $f(\mathcal{R})$ and $g(\mathcal{R})$ on the ratio between the annular pore radii $\mathcal{R}=R_i/R$. The analytical results are shown in continuous [Eq. (42)] and dashed [Eq. (44)] black lines. FEM calculations are shown with markers. Circles: $\mathcal{K}_0/\mathcal{K}_0(\mathcal{R}=0)$. Crosses: $\theta_0/\theta_0(\mathcal{R}=0)$. Squares: $\Lambda/\Lambda(\mathcal{R}=0)$. The inset plot shows the permeability ratios (a) $\mathcal{K}_0/\mathcal{K}_0^{slit}$ and (b) $\mathcal{K}_0/\mathcal{K}_0^{rect}$ as a function of $\mathcal{R}$ (see the main text for more details).

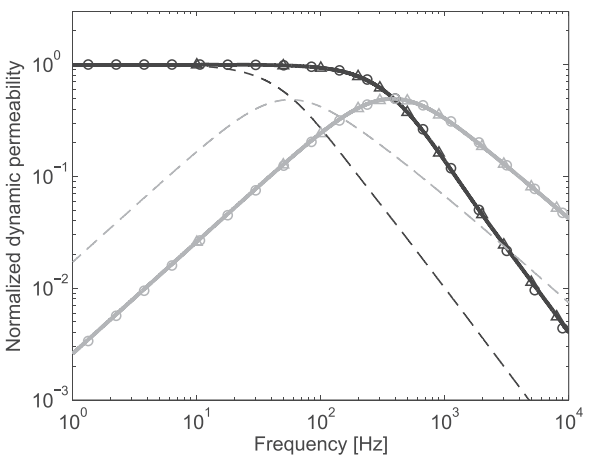

FIG. 3. Normalized dynamic viscous permeability of an array of annular pores with $R=500\,\mu$m, $\mathcal{R}=0.5$, and $\phi=0.3$. Continuous lines: analytical model. Circles: semi-phenomenological model. Triangles: direct numerical simulation (FEM). Dashed lines: analytical model for an array of cylindrical pores (with $R=500\,\mu$m and $\phi=0.3$). Black: $\mathrm{Re}(\mathcal{K}(\omega)/\mathcal{K}_0)$. Gray: $-\mathrm{Im}(\mathcal{K}(\omega)/\mathcal{K}_0)$.

Figure 4 shows the normalized bulk modulus of an array of annular pores with the same parameters as those in Fig. 3. This has been calculated using Eq. (35) and the analytical expression for the dynamic thermal permeability given by Eq. (36). As in Fig. 3, this is compared with both the dynamic bulk modulus obtained by using the semi-phenomenological model Eqs. (47) and the parameters derived in Sec. II B, and its direct numerical calculation obtained from the solution of Eqs. (11) and (13) for a discrete set of frequencies. An excellent agreement is observed between the calculations obtained with the different models. On the other hand, the real part of the dynamic bulk modulus of the array of annular pores is smaller than that of an array of cylindrical pores with the same value of R and ϕ. This, along with the smaller permeability, leads to a slower speed of sound and larger attenuation at low frequencies, as shown in the inset plots of Fig. 4 and predicted by Eq. (49).

B. Experimental validation

The analytical model introduced in Sec. II A is now validated by comparing its predictions with measured normal incidence sound absorption coefficient data published in Ref. 7. The measured samples comprises 25-mm-depth brass disks with multiple cylindrical holes of radius R ranging from 4 down to 1 mm. Annular pores of various width $w = R(1-\mathcal{R})$ were created by introducing stainless steel round rods in the holes. The rods have different radius R_i ranging from 0.75 to 2.0 mm. Measurements of materials without the rods (i.e., array of cylindrical pores) were also presented in Ref. 7. For both type of arrays, the measurements were taken in a Brüel & Kjær type 4206-2 impedance tube with an internal diameter of 29 mm by following the measurement procedure described in Ref. 23 and spanning the frequency range 500–6400 Hz for which any local characteristic size is much smaller than the wavelength.

Figure 5 shows the normal incidence sound absorption coefficient α of rigidly backed arrays of annular pores with

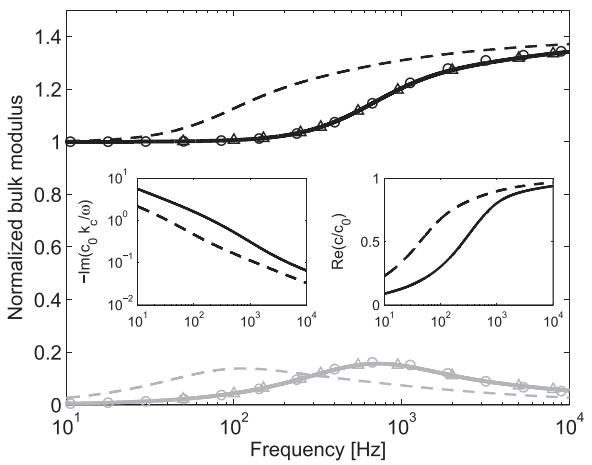

FIG. 4. Normalized dynamic bulk modulus of an array of annular pores with $R = 500\,\mu$m, $\mathcal{R} = 0.5$, and $\phi = 0.3$. Continuous lines: analytical model. Circles: semi-phenomenological model. Triangles: direct numerical simulation (FEM). Dashed lines: analytical model for an array of cylindrical pores (with $R = 500\,\mu$m and $\phi = 0.3$). Main plot—Black: $\mathrm{Re}(\phi E(\omega)/P_0)$. Gray: $\mathrm{Im}(\phi E(\omega)/P_0)$. Right inset plot—normalized speed of sound $\mathrm{Re}(\mathcal{C}(\omega)/c_0)$. Left inset plot—normalized attenuation coefficient $-\mathrm{Im}(c_0 k_c(\omega)/\omega)$.

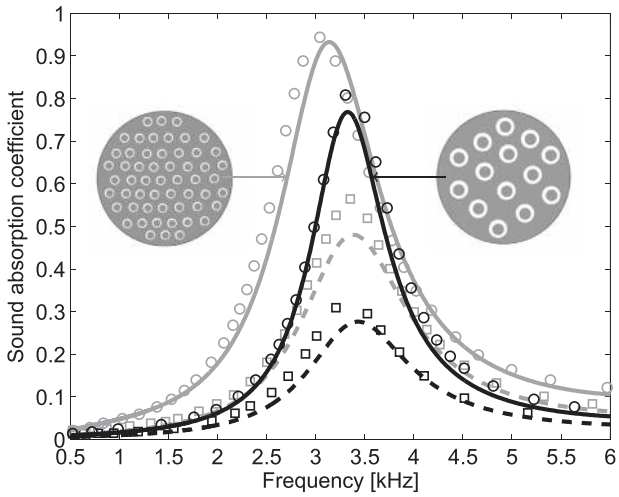

FIG. 5. Predicted (lines) and measured (markers) normal incidence sound absorption coefficient of a rigidly backed 25-mm layer of material. Arrays of annular pores with $R = 1$ mm, $R_i = 0.75$ mm, and $\phi = 0.1144$ (continuous gray line) and $R = 2$ mm, $R_i = 1.25$ mm, and $\phi = 0.1623$ (continuous black line). Array of cylindrical pores (i.e., $R_i = 0$) with $R = 1$ mm and $\phi = 0.2616$ (dashed gray line) and with $R = 2$ mm and $\phi = 0.2663$ (dashed black line). The experimental data were taken from Ref. 7.

parameters $R = 1$ mm, $R_i = 0.75$ mm, and $\phi = 0.1144$; and $R = 2$ mm, $R_i = 1.25$ mm, and $\phi = 0.1623$. The porosity has been calculated as $\phi = NR^2(1-\mathcal{R}^2)/R_{tube}^2$, where N is the number of annular pores and R_{tube} is the radius of the impedance tube. The material thickness is 25 mm. Note that α for arrays of cylindrical pores (i.e., $R_i = 0$) is also plotted. A good agreement between the predictions of the model introduced in the present work and the experimental data published in Ref. 7 is obtained. A similar level of agreement has been found in Ref. 7 using a model for slit pores and a corrected layer thickness. This is because the radii ratio takes values $\mathcal{R} = 0.75$ and $\mathcal{R} = 0.625$ for the materials whose α is displayed in Fig. 5. As discussed in Sec. III A, materials with annular pores and radii ratio values larger than approximately 0.5 possess similar acoustical properties than those of materials with slit pores with width $2h = w$ and the same porosity. On the other hand, it is worth mentioning that our model provides a good agreement between predictions and data for the other materials tested in Ref. 7. However, this is not shown for the sake of brevity. The model introduced in this work can be considered as validated.

C. Parametric analysis

A parametric analysis of the microstructure parameters influencing the sound absorptive properties of porous materials with annular pores is presented in this section. Figure 6 shows the influence of porosity ϕ on normal incidence sound absorption coefficient α for arrays of annular and cylindrical pores. For the former, the following parameters are considered $\mathcal{R} = 0.5$ and $R = 250\,\mu$m, while for the latter the same value of R is used for the cylindrical pore radius. Two porosity values are considered, i.e., $\phi = 0.3$ and $\phi = 0.6$, and a layer thickness of 25 mm. The static flow resistivity values are $\sigma_0(\phi = 0.3) = 46.6579$, $\sigma_0(\phi = 0.6) = 23.3290$, $\sigma_0(\phi = 0.3, \mathcal{R} = 0) = 7.8375$, and $\sigma_0(\phi = 0.6, \mathcal{R} = 0) = 3.9188\,\mathrm{kPa\,s/m^2}$. The sound absorption

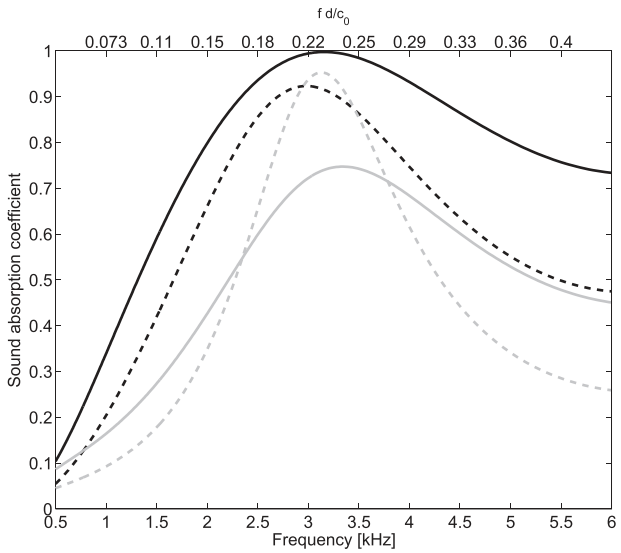

FIG. 6. Influence of porosity on normal incidence sound absorption coefficient of a rigidly backed 25-mm thick array of annular (black lines) and cylindrical (gray lines) pores with porosity $\phi = 0.6$ (continuous lines) and $\phi = 0.3$ (dashed lines). The other parameters are $R = 250\,\mu$m and $\mathcal{R} = 0.5$.

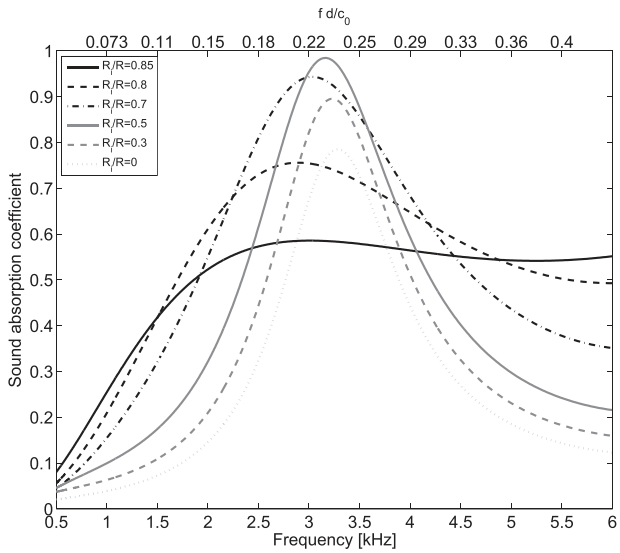

FIG. 7. Influence of the radius ratio $\mathcal{R} = R_i/R$ on normal incidence sound absorption coefficient α of a rigidly backed 25-mm thick layer of porous materials with annular pores with porosity $\phi = 0.25$ and $R = 500\,\mu$m. The α values for an array of cylindrical pores (i.e., $\mathcal{R} = 0$) are also plotted for comparison.

coefficient of materials with small porosity values shows a pronounced peak approximately located at a frequency $c_0/4d$. For materials with larger porosity, the sound waves can penetrate the material further leading to stronger generation of viscous stresses and thermal exchanges between the solid and the saturating fluid. This results in higher sound attenuation. Consequently, the sound absorption coefficient can approach its maximum value and its peak becomes wider. As shown in the figure, a porous material with annular pores can present higher sound absorption coefficient values than that of a porous material having cylindrical pores with the same porosity ϕ and pore radius R. This is caused by the larger sound attenuation exhibited by the former type of materials, as illustrated in Fig. 4. In turn, the larger attenuation is a consequence of the smaller (respectively, larger) real (respectively, imaginary) part of the bulk modulus as well as the larger real part of the dynamic flow resistivity, which is defined as $\sigma(\omega) = \eta/\mathcal{K}(\omega)$. However, it must be emphasized that for smaller values of R the opposite trend can be observed.

Figure 7 shows the influence of the radius ratio $\mathcal{R} = R_i/R$ (or that of the inner radius R_i for a constant outer radius R) on the normal incidence sound absorption coefficient α of arrays of annular pores with porosity $\phi = 0.25$ and $R = 500\,\mu$m. In this case, the static flow resistivity of the materials varies from $\sigma_0(\mathcal{R}=0) = 2.3513$ up to $\sigma_0(\mathcal{R}=0.85) = 156.6818\,\mathrm{kPa\,s/m^2}$. For materials with large values of $\mathcal{R}$ the viscous (and thermal) boundary layer thickness approaches the characteristic size of the annular pores in the frequency range under consideration. As a consequence, the sound absorption coefficient displays a broadband behavior. As $\mathcal{R}$ decreases, a transition from the broadband behavior to one where a pronounced absorptive peak located approximately at a frequency $c_0/4d$ is observed. This transition for the material considered in Fig. 7 occurs at a value of approximately $\mathcal{R} = 0.6$, which corresponds to a static flow resistivity of $21.9485\,\mathrm{kPa\,s/m^2}$. For this value, the amplitude of the absorptive peak reaches a maximum value. As previously, for smaller values of R, an array of cylindrical pores can exhibit larger sound absorption coefficient than that of a porous material with annular pores.

Figures 8 shows the influence of the radius R on the normal incidence sound absorption coefficient α of a rigidly backed 25-mm-thick layer of a porous material with annular pores. The porosity and the radius ratio have been set to $\phi = 0.3$ and $\mathcal{R} = 0.6$, respectively. The flow resistivity varies from $\sigma_0(R = 50\,\mu\mathrm{m}) = 1.829\,\mathrm{MPa\,s/m^2}$ down to $\sigma_0(R = 1250\,\mu\mathrm{m}) = 2.9265\,\mathrm{kPa\,s/m^2}$. Two distinctive type of behavior are observed depending on the values of R. For small values of R (or large flow resistivity), the sound absorption coefficient of materials with annular pores does not present a marked peak but rather a broadband behavior, while for larger values of R (or small flow resistivity), it displays a pronounced peak approximately located at a frequency of approximately $c_0/4d$. As mentioned previously, arrays of annular pores with small values of R can provide lower sound absorption coefficient values than that of arrays of cylindrical pores with the same porosity and pore radius R. The opposite trend is found for larger values of R.

The influence of the sample thickness on the normal incidence absorption coefficient of porous materials with annular pores is rather conventional, i.e., thicker materials provide larger sound absorption coefficient α. This trend is observed up to a critical thickness value for which α is no longer substantially increased.[20] Such a critical thickness value is smaller for materials with larger flow resistivity (i.e., material with small values of R and porosity, and/or large values of $\mathcal{R}$). In addition, since the first absorptive peak is characterized by the quarter-wavelength condition $d = \lambda/4$, thicker materials display this peak at lower frequencies. Unfortunately, no simple expression relating the amplitude of this peak to the microstructural parameters of the materials could be found. The reason for this is that the acoustical properties of materials with annular pores cannot

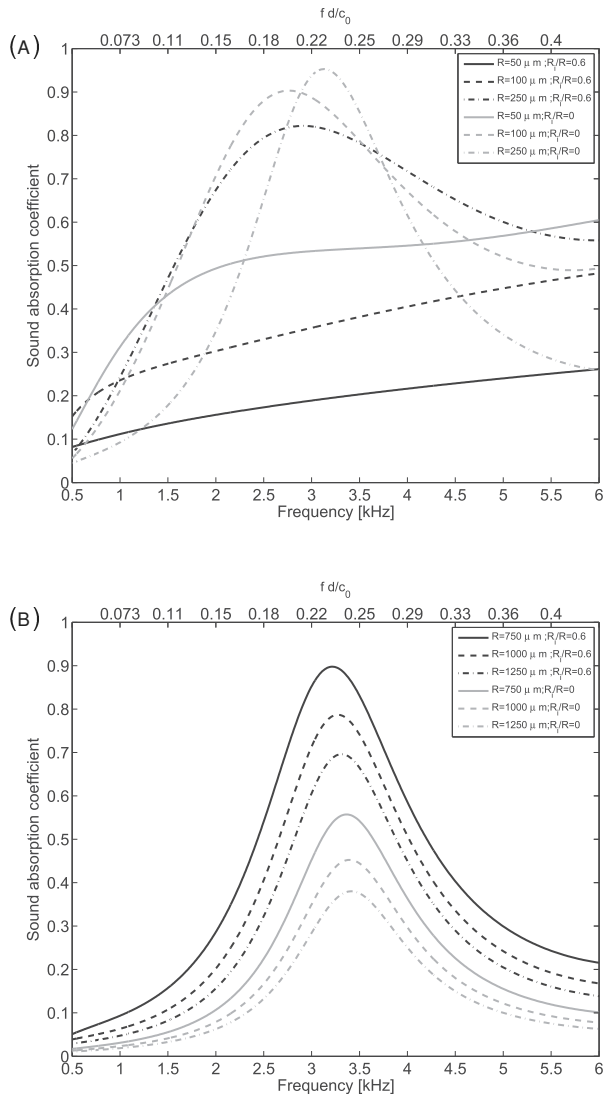

FIG. 8. Influence of the radius R on normal incidence sound absorption coefficient α of a rigidly backed 25-mm thick layer of a porous material with annular pores with porosity $\phi = 0.3$ and $\mathcal{R} = 0.6$. The α values for an array of cylindrical pores (i.e., $\mathcal{R} = 0$) are also plotted for comparison.

be approximated by their simple limiting low- or high-frequency values in the frequency region around the first absorptive peak.

IV. CONCLUSIONS

This paper investigated long-wavelength sound propagation in porous materials with annular pores. We have introduced closed-form analytical expressions for the long-wavelength effective acoustical properties of this type of material. These have been successfully compared with those calculated with semi-phenomenological models and direct numerical simulations. The introduced model has been validated by comparing its predictions with measured data published in Ref. 7.

A parametric analysis of the geometrical descriptors of the materials have revealed that the sound absorption coefficient of porous materials with annular pores could show pronounced peak or broadband behavior. This type of materials can provide higher sound absorption than that achieved by arrays of cylindrical pores with the same porosity and pore radius equal to the annular pore outer radius. Such a trend is particularly strong when the annular pore outer radius is relatively large.

Other potential applications of the results presented in this work may include (i) the modeling of the acoustical properties of biomass tubules since their inner geometry resembles that of annular pores[24] and (ii) inverse methods for pipe monitoring[25] where the introduced long-wavelength effective properties may be used in conjunction with pulse reflectometry applied in the region of plane wave propagation to assess pipe blockage. In addition, our model can be extended to investigate the thermoacoustic properties[26] of porous materials with annular pores.

ACKNOWLEDGMENTS

R.V. gratefully acknowledges support from the project METAUDIBLE (Grant No. ANR 13-BS09-0003-03), co-funded by the Agence Nationale de la Recherche (ANR) and Fondation de Recherche pour l'Aéronautique et l'Espace (FRAE), and CeLyA of Université de Lyon.

[1]G. Kirchhoff, "Ueber den Einfluss der Wirmeleitung in einem Gase auf die Schallbewegung" ("About the influence of heat conduction on the sound propagation in a gas"), Ann. Phys. **210**, 177–193 (1868).
[2]C. Zwikker and C. W. Kosten, *Sound Absorbing Materials* (Elsevier, Amsterdam, 1949), pp. 1–174.
[3]H. Tijdeman, "On the propagation of sound waves in cylindrical tubes," J. Sound Vib. **39**, 1–33 (1975).
[4]M. R. Stinson, "The propagation of plane sound waves in narrow and wide circular tubes, and generalization to uniform tubes of arbitrary cross-sectional shape," J. Acoust. Soc. Am. **89**, 550–558 (1991).
[5]J. L. Auriault, C. Boutin, and C. Geindreau, *Homogenization of Coupled Phenomena in Heterogeneous Media* (Wiley, London, 2009), pp. 1–472.
[6]D. E. Weston, "The theory of the propagation of plane sound waves in tubes," Proc. Phys. Soc. London Sec. B **66**, 695–709 (1953).
[7]S. Sakamoto, A. Nakano, H. Tanikawa, and Y. Maruyama, "Estimation and experiment for sound absorption coefficient of cross-sectional shape of clearance by concentric cylinder," J. Adv. Mech. Des. Syst. **9**(3), 1–13 (2015).
[8]D. L. Johnson, J. Koplik, and R. Dashen, "Theory of dynamic permeability and tortuosity in fluid-saturated porous media," J. Fluid Mech. **176**, 379–402 (1987).
[9]Y. Champoux and J. F. Allard, "Dynamic tortuosity and bulk modulus in air-saturated porous media," J. Appl. Phys. **70**(4), 1975–1979 (1991).
[10]D. Lafarge, P. Lemarinier, J. F. Allard, and V. Tarnow, "Dynamic compressibility of air in porous structures at audible frequencies," J. Acoust. Soc. Am. **102**(4), 1995–2006 (1997).
[11]S. Tsangaris, "Oscillatory flow of an incompressible viscous fluid in a straight annular pipe," J. Mech. Theor. Appl. **3**, 467–478 (1984).
[12]E. Rukmangadachari, "Dusty viscous flow through a cylinder of triangular cross-section," Proc. Math. Sci. **88**(2), 169–179 (1979).
[13]C. Y. Wang, "Analytic solutions for pulsatile flow through annular, rectangular and sector ducts filled with a Darcy-Brinkman medium," Transp. Porous Med. **112**(2), 409–428 (2016).
[14]B. S. Mazumder and K. K. Modal, "On solute transport in oscillatory flow through an annular pipe with a reactive wall and its application to a catherized artery," Quart. J. Mech. Appl. Math **58**(3), 349–365 (2005).
[15]P. N. Shankar, "Acoustic refraction and attenuation in cylindrical and annular ducts," J. Sound. Vib. **22**(2), 233–246 (1972).
[16]V. V. Golubev and H. M. Attasi, "Sound propagation in an annular duct with mean potential swirling flow," J. Sound. Vib. **198**(5), 601–616 (1996).
[17]F. Hunt, "Notes on the exact equations governing the propagation of sound in fluids," J. Acoust. Soc. Am. **27**, 1019–1039 (1955).
[18]V. F. Kozlov, A. V. Fedorov, and N. D. Malmuth, "Acoustic properties of rarefied gases inside pores of simple geometries," J. Acoust. Soc. Am. **117**, 3402–3411 (2005).

[19]O. Umnova, D. Tsiklauri, and R. Venegas, "Effect of boundary slip on the acoustical properties of microfibrous materials," J. Acoust. Soc. Am. **126**(4), 1850–1861 (2009).
[20]R. Venegas, "Microstructure influence on acoustical properties of multiscale porous materials," Ph.D. thesis, University of Salford, Salford, UK, 2011.
[21]M. Abramowitz and I. A. Stegun, *Handbook of Mathematical Functions with Formulas, Graphs, and Mathematical Tables* (Dover, New York, 1972), Chaps. 9 and 10.
[22]J. F. Allard and N. Atalla, *Propagation of Sound in Porous Media: Modelling Sound Absorbing Materials* (Wiley, West Sussex, 2009), pp. 1–372.
[23]ISO 10534-2:2001, "Acoustics–Determination of sound absorption coefficient and impedance in impedance tubes–Part 2: Transfer-function method" (International Organization for Standardization, Geneva, Switzerland, 2001).
[24]S. Sakamoto, Y. Takauchi, K. Yanagimoto, and S. Watanabe, "Study for sound absorbing materials of biomass tubule etc. (Measured result for rice straw, rice husks, and buckwheat husks)," J. Env. Eng. **6**(2), 352–364 (2011).
[25]W. Duan, R. Kirby, J. Prisutova, and K. V. Horoshenkov, "On the use of power reflection ratio and phase change to determine the geometry of a blockage in a pipe," Appl. Acoust. **87**, 190–197 (2015).
[26]W. Pat Arnott, H. Bass, and R. Raspet, "General formulation of thermoacoustics for stacks having arbitrarily shaped pore cross sections," J. Acoust. Soc. Am. **90**, 3228–3237 (1991).